Acta Geophysica
https://doi.org/10.1007/s11600-018-0148-8

RESEARCH ARTICLE - APPLIED GEOPHYSICS

An improved grey wolf optimizer algorithm for the inversion of geoelectrical data

Si-Yu Li[1] · Shu-Ming Wang[1] · Peng-Fei Wang[1] · Xiao-Lu Su[1] · Xin-Song Zhang[2] · Zhi-Hui Dong[1]

Received: 30 October 2017 / Accepted: 11 April 2018

Abstract
The grey wolf optimizer (GWO) is a novel bionics algorithm inspired by the social rank and prey-seeking behaviors of grey wolves. The GWO algorithm is easy to implement because of its basic concept, simple formula, and small number of parameters. This paper develops a GWO algorithm with a nonlinear convergence factor and an adaptive location updating strategy and applies this improved grey wolf optimizer (improved grey wolf optimizer, IGWO) algorithm to geophysical inversion problems using magnetotelluric (MT), DC resistivity and induced polarization (IP) methods. Numerical tests in MATLAB 2010b for the forward modeling data and the observed data show that the IGWO algorithm can find the global minimum and rarely sinks to the local minima. For further study, inverted results using the IGWO are contrasted with particle swarm optimization (PSO) and the simulated annealing (SA) algorithm. The outcomes of the comparison reveal that the IGWO and PSO similarly perform better in counterpoising exploration and exploitation with a given number of iterations than the SA.

Keywords Grey wolf optimizer · Improved grey wolf optimizer · Geoelectrical · Geoelectrical methods · Inversion

Introduction

In recent decades, electrical and electromagnetic methods such as DC resistivity, induced polarization (IP) and magnetotelluric (MT) methods have received attention from researchers for many applications in groundwater management; geothermal resources, and oil, gas, and mineral-deposit exploration (Nabighian and Asten 2002; Simpson and Bahr 2005; Zhdanov 2010).

The inversion and interpretation of the observed data are considered among the greatest challenges of geophysical methods. Geophysical inversion problems are typically highly nonlinear, multi-minimum and discontinuous. Therefore, all linearized inversion strategies, such as the generalized-inverse (GI) method (Smith and Franklin 1969) and Levenberg–Marquardt (LM) method (Davis 1993), are susceptible to dropping into local optimums. These linearized methods also heavily depend on the initial model.

Dissimilarly, nonlinear bionic methods for geophysical inversion problems have various advantages: they are highly efficient, have a good convergence speed, and do not require a reasonable initial model. In recent years, this type of algorithm has been actively applied in the geophysical field for resolving optimization inverse problems; examples include the genetic algorithm (GA) (Parolai et al. 2005; Sen and Stoffa 1992; Shi et al. 2000; Wang and Tan 2005), simulated annealing (SA) (Dosso and Oldenburg 1991; Wang et al. 2012; Yang et al. 2002), particle swarm optimization (PSO) (Dos Santos Coelho and Alotto 2008; Mikki and Kishk 2005; Shaw and Srivastava 2007), colony optimization (Chen et al. 2005; Dorigo and Stützle 2003; Wang et al. 2009), glowworm swarm optimization (GSO) (Krishnanand and Ghose 2006; Krishnanand 2007; Mo et al. 2016), gravitational search algorithm (GSA) (Rashedi

✉ Shu-Ming Wang
whwsm@hotmail.com

[1] Hubei Subsurface Multi-scale Imaging Key Laboratory, Institute of Geophysics and Geomatics, China University of Geosciences, Wuhan 430074, China

[2] State Key Laboratory of Biogeology and Environmental Geology, School of Earth Sciences, China University of Geosciences, Wuhan 430074, China

Published online: 10 May 2018

et al. 2009), bat algorithm (Yang and Hossein Gandomi 2012; Yang 2010; Yang 2011), fruit fly optimization algorithm (FOA) (Pan 2012), ant lion optimizer (ALO) (Mirjalili 2015a), and multi-verse optimizer (MVO) (Mirjalili et al. 2016).

The grey wolf optimizer (GWO) algorithm presented by Mirjalili et al. (2014) is a novel bionics algorithm inspired by the social rank and prey-seeking behavior of grey wolves in nature.

Recently, the grey wolf optimizer (GWO) has been utilized in engineering optimization and other scientific computation fields. Sulaiman et al. (2015) have shown the effectiveness of the GWO in an optimal reactive power dispatch problem using two bus-system case studies. Mirjalili (2015b) has proven that the GWO can provide highly competitive results in multi-layer perceptron (MLP) problems. Kamboj et al. (2016) have applied the GWO algorithm to solve economic load dispatch problems. Song et al. (2015) have applied the GWO algorithm to surface wave dispersion curve inversion problems. Modified schemes for improving the original GWO algorithm were recently proposed by hybridizing the GWO with differential algorithms (Chahar and Kumar 2017; Heidari and Pahlavani 2017; Jadhav and Gomathi 2017; Zhu et al. 2015), or by incorporating different convergence factor formulas to focus on an appropriate balance between exploration and exploitation (Mittal et al. 2016; Mohamed et al. 2015; Muangkote et al. 2014).

In this paper, the GWO algorithm is improved by a nonlinear convergence factor and an adaptive location updating strategy. The applicability of the improved grey wolf optimizer (IGWO) algorithm to geophysical inverse problems is tested using MT, DC and IP data. Furthermore, the above results are compared to the results of PSO and SA to further test the performance of the IGWO. The comparison illustrates that the IGWO algorithm effectively balances the global exploration and local exploitation, helping to find a highly accurate solution.

Grey wolf optimizer

The GWO, as a recently presented algorithm, imitates the social rank and prey-seeking behaviors of grey wolves. Members of a grey wolf pack are stratified according to the following four ranks: alpha (α), beta (β), delta (δ) and omega (ω).

Social hierarchy

The social structure of a grey wolf pack has very strict levels of hierarchy that must be adhered to by all members of the pack. The leader of a grey wolf pack is the alpha (α). As the commander of the whole pack, the alpha is responsible for the decisions governing certain daily activities. The second level is beta (β), which is only submissive to the commander. The delta (δ), as the third level, is under the command of the upper ranks. The others are omegas (ω). Omegas are at the bottom of the hierarchy and must obey other dominant wolves, playing the role of maintaining the dominance structure and balancing the entire wolf pack. A model of grey wolves' social hierarchy is pictured in Fig. 1.

Apart from the grey wolves' social hierarchy, their prey-seeking activity is also simulated in the GWO algorithm. There are three different stages in their hunting activity (Muro et al. 2011):

1. Following the trail of the prey and getting close to the prey;
2. Surrounding the prey and forcing the prey to stop moving;
3. Assaulting the prey.

Following the trail of the prey, and getting close to the prey

The alpha is the leader of the grey wolf pack and all the other wolves are under the command of the alpha. In the GWO algorithm, alpha represents the fittest solution. Omegas must submit to the upper three ranks. The corresponding equations are proposed (Mirjalili et al. 2014):

$$\boldsymbol{D} = \left|\boldsymbol{C} \cdot \boldsymbol{x}_p(t) - \boldsymbol{x}(t)\right|, \tag{1}$$

$$\boldsymbol{x}(t+1) = \boldsymbol{x}_p(t) - \boldsymbol{A} \cdot \boldsymbol{D}, \tag{2}$$

t symbolizes the number of iterations; $\cdot$ indicates a dot product; $\boldsymbol{x}_p$ indicates the location of the prey; $\boldsymbol{x}$ indicates the location of a grey wolf; and $\boldsymbol{C}$ and $\boldsymbol{A}$ represent two searching coefficient vectors:

$$\boldsymbol{A} = 2\boldsymbol{a} \cdot \boldsymbol{r}_1 - \boldsymbol{a}, \tag{3}$$

$$\boldsymbol{C} = 2\boldsymbol{r}_2, \tag{4}$$

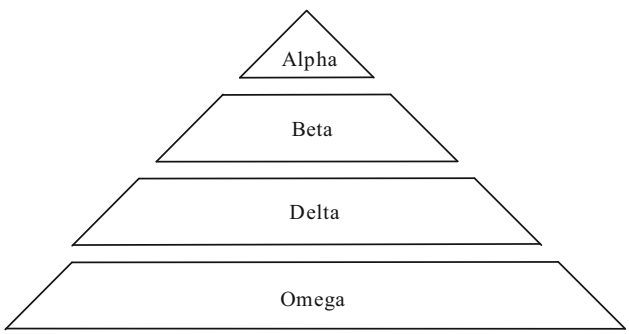

Fig. 1 Model of the social hierarchy of the grey wolf

Fig. 2 Pseudo-code of the GWO algorithm

```
Initialize the population of the grey wolf: N, the maximum iterations t_max, A, C, a;
Initialize the grey wolf x_i (i=1,2,...,N);
For each wolf, calculate the fitness value;
Rank the wolf pack as alpha (α), beta (β), delta (δ) and omegas (ω);
for t=1:1:t_max
    for each omega (ω)
        Update the position by equations (5)-(8);
    end for
    Obtain the updated wolf pack;
    Update A, C and a;
    Recalculate the fitness values of the wolves;
    Rank the updated wolf pack as alpha (α), beta (β), delta (δ) and omegas (ω);
end for
Return the position of alpha (α) as the final solution.
```

where $\boldsymbol{a}$ is linearly diminished in $[0, 2]$ and $\boldsymbol{r}_1$ and $\boldsymbol{r}_2$ are random value vectors in $[0, 1]$.

Surrounding the prey, and forcing the prey to stop moving

In the hunting procedure, the prey is regarded as an optimal solution and the alpha possesses the best ability to follow the trail of the prey. Considering the uncertainty of the real location of the prey in a geophysical inverse problem, alpha is assumed as the location of the prey because it is closest to the prey.

Omegas update their locations via the guidance of the other three wolves. Grey wolves split up to chase the prey separately and then they move towards each other to assault. The corresponding formulas are proposed (Mirjalili et al. 2014):

$$\begin{cases} \boldsymbol{D}_\alpha = |\boldsymbol{C}_1 \boldsymbol{x}_\alpha(t) - \boldsymbol{x}(t)| \\ \boldsymbol{D}_\beta = |\boldsymbol{C}_2 \boldsymbol{x}_\beta(t) - \boldsymbol{x}(t)| \\ \boldsymbol{D}_\delta = |\boldsymbol{C}_3 \boldsymbol{x}_\delta(t) - \boldsymbol{x}(t)|, \end{cases} \tag{5}$$

where $\boldsymbol{C}_i = 2 \times r_{i1}$, r_{i1} is a random vector in $[0, 1]$, and $i = 1, 2, 3$.

$$\begin{cases} \boldsymbol{x}_1 = \boldsymbol{x}_\alpha(t) - \boldsymbol{A}_1 \cdot \boldsymbol{D}_\alpha \\ \boldsymbol{x}_2 = \boldsymbol{x}_\beta(t) - \boldsymbol{A}_2 \cdot \boldsymbol{D}_\beta \\ \boldsymbol{x}_3 = \boldsymbol{x}_\delta(t) - \boldsymbol{A}_3 \cdot \boldsymbol{D}_\delta, \end{cases} \tag{6}$$

$$\boldsymbol{x} = (\boldsymbol{x}_1 + \boldsymbol{x}_2 + \boldsymbol{x}_3)/3, \tag{7}$$

where

$$\boldsymbol{A}_i = 2\boldsymbol{a} \cdot r_{i2} - \boldsymbol{a}, \tag{8}$$

where r_{i2} is a random vector in $[0, 1]$ and $\boldsymbol{x}_\alpha(t)$, $\boldsymbol{x}_\beta(t)$ and $\boldsymbol{x}_\delta(t)$ indicate the locations of alpha, beta and delta, respectively, at the iteration of t.

Assaulting the prey

According to Eq. (3), with the linear decrease of $\boldsymbol{a}$, $\boldsymbol{A}$ is variable between -2 and 2. In the initial stage of iteration, $|\boldsymbol{A}| > 1$, and the prey can be in any place; therefore, the grey wolf pack will expand the encircling circle and the global exploration is dominant. In the later iterative period, $|\boldsymbol{A}| < 1$, and the local exploitation is dominant; therefore, the encircling circle will shrink to a reasonable size and the candidate solutions converge towards the position of the prey. The pseudo-code of the GWO is provided in Fig. 2.

Improved grey wolf optimizer

In terms of the characteristics of the geophysical inverse problems, we improve the original GWO algorithm to ensure its performance in the geophysical inversion problems. On one hand, an improved convergence factor is proposed to adapt to the nonlinear inverse problems. On the other hand, equations of the conventional location updating strategy are modified in terms of the differences between the individual fitness values of alpha, beta, and delta. This modified GWO algorithm is proposed as the IGWO.

Nonlinear convergence factor

The convergence factor $\boldsymbol{a}$ in the GWO algorithm linearly varies from 2 to 0. In this paper, the equation of the convergence factor is modified as follows for a better balance between exploration and exploitation:

$$\boldsymbol{a} = 2\left(1 - \left(\frac{t-1}{t_{max}-1}\right)^{1.5}\right). \tag{9}$$

In Eq. (9), the convergence factor $\boldsymbol{a}$ is described as an exponential variation, as shown in Fig. 3. In the original GWO algorithm, half of the iterations are for exploration

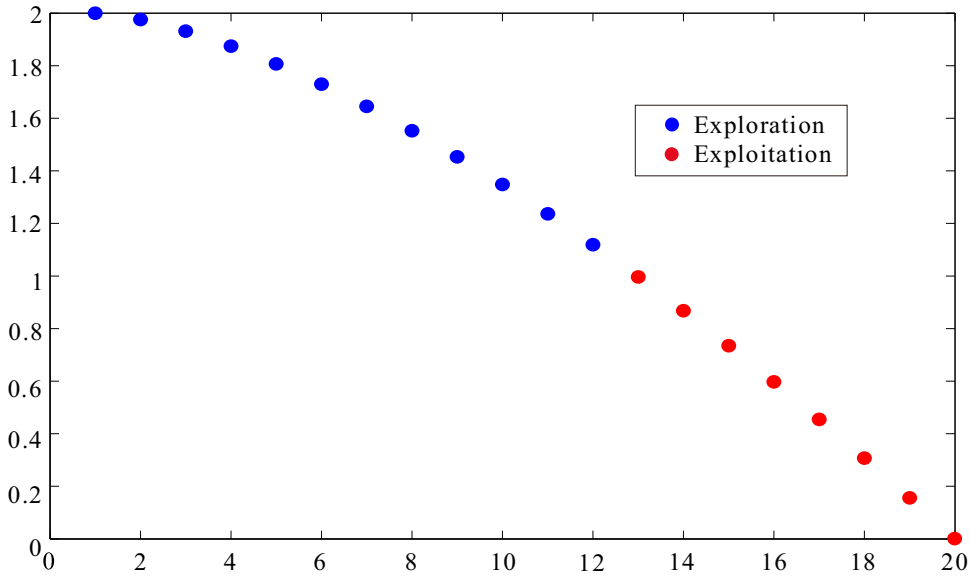

Fig. 3 Modified convergence factor (when the maximum iteration is 20)

Table 1 Results for the multi-extrema function tests

Function	Number of dimensions	Optimum	Search space	Number of iterations required	
				IGWO	GWO
F_1	1	0	$-1000 \leq x \leq 1000$	14	27
F_2	2	[0, 0]	$-500 \leq x, y \leq 500$	21	30
F_3	3	[0, 0, 0]	$-2000 \leq x, y, z \leq 2000$	130	662

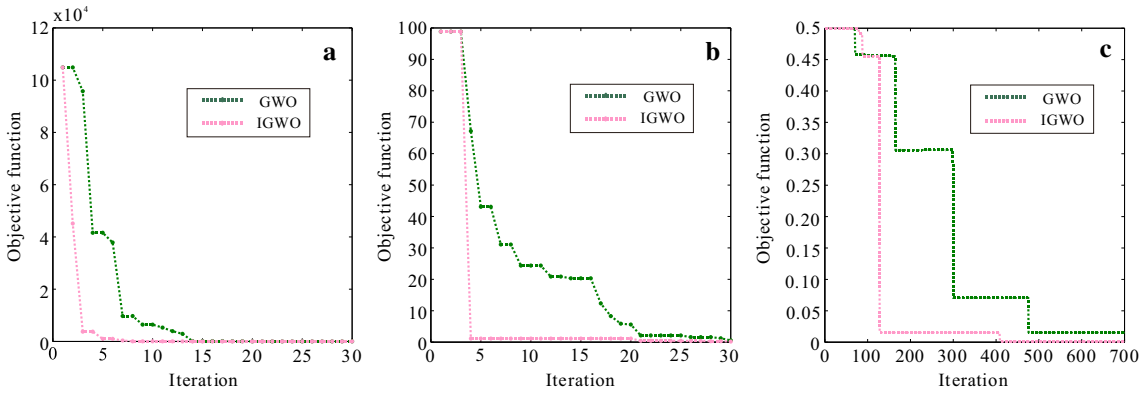

Fig. 4 Fitness behaviors of the GWO and IGWO. **a** Objective values in the test using F_1. **b** Objective values in the test using F_2. **c** Objective values in the test using F_3

and the other half are devoted to exploitation. With the modified convergence factor, a larger number of iterations are used for exploration, which is beneficial to avoid the local minima. Using this type of nonlinear convergence factor, the percentage of iterations used for exploration and exploitation is approximately 60 and 40%, respectively.

Weighted location updating strategy

The conventional location updating strategy of omegas is calculated via Eqs. (5), (6) and (7). According to Eqs. (5), (6) and (7), alpha, beta and delta are equally important for the updating position of omegas. Thus, the location updating strategy in the original GWO loses sight of the vital differences for the three upper social ranks.

Here, an improved location updating strategy is proposed:

$$\begin{cases} Q(\alpha) = 1/\Psi(\boldsymbol{x}_\alpha(t)) \\ Q(\beta) = 1/\Psi(\boldsymbol{x}_\beta(t)) \\ Q(\delta) = 1/\Psi(\boldsymbol{x}_\delta(t)) \end{cases}, \tag{10}$$

$$\begin{aligned} \boldsymbol{x} = {} & \boldsymbol{x}_\alpha \cdot [Q(\alpha)/(Q(\alpha) + Q(\beta) + Q(\delta))] \\ & + \boldsymbol{x}_\beta \cdot [Q(\beta)/(Q(\alpha) + Q(\beta) + Q(\delta))] \\ & + \boldsymbol{x}_\delta \cdot [Q(\delta)/(Q(\alpha) + Q(\beta) + Q(\delta))], \end{aligned} \tag{11}$$

where Ψ represents the object function; Q is described as the inverse of Ψ; and $Q(\alpha)$, $Q(\beta)$ and $Q(\delta)$ are fitness values of alpha, beta and delta, respectively, at the current iteration t.

In the original GWO, the ratios for the three best wolves guiding omegas to update their positions are equal and this searching strategy seems to ignore the differences among alpha, beta and delta. The adaptive searching strategy controls the searching direction by the fitness values of alpha, beta and delta and improves the convergence speed and the optimization precision. Equations (10) and (11) reveal the improved principle of searching strategies: alpha tends to play a greater role in guiding the direction and step length of omegas' updated positions than does beta, while beta tends to play a greater role in guiding the direction and step length of omegas' updated positions than does delta.

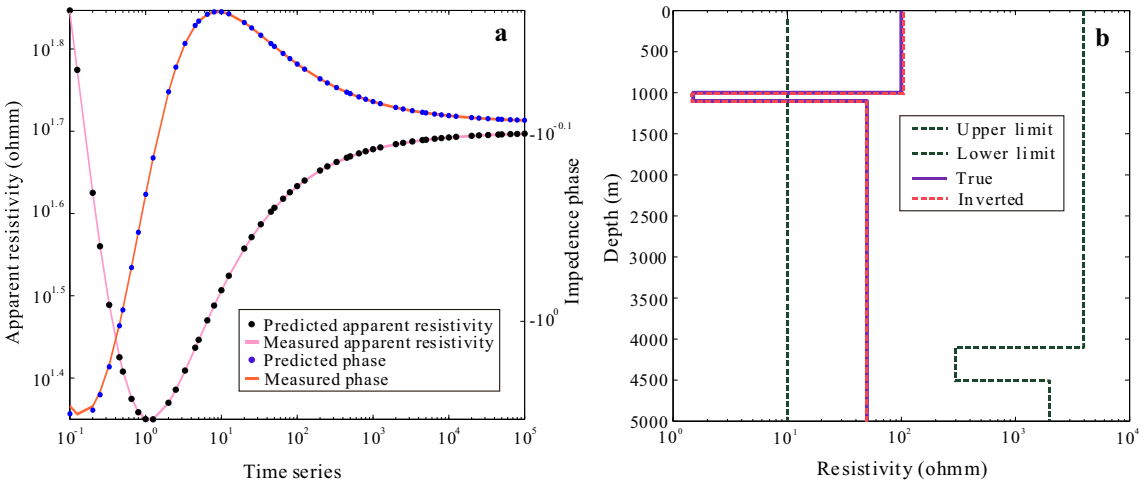

Fig. 5 Inverted results using the IGWO based on noiseless forward modeling data from model A. **a** The measured apparent resistivity and phase and the predicted apparent resistivity and phase using the IGWO. **b** The search area, inversion solution and true model

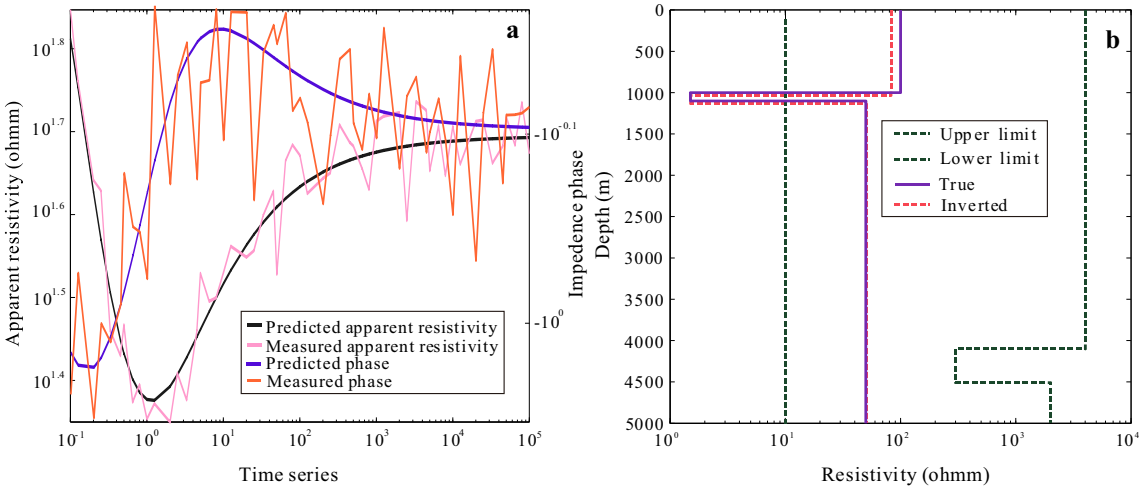

Fig. 6 Inverted results using the IGWO based on the data from model A with 10% noise. **a** The noisy measured apparent resistivity and phase and the predicted apparent resistivity and phase using the IGWO. **b** The search area, inversion solution and true model

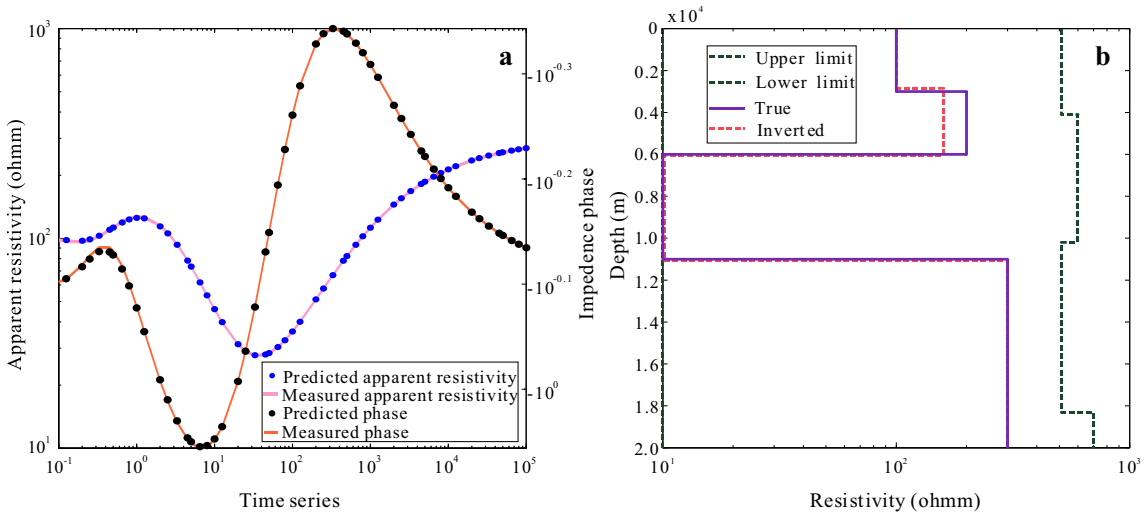

Fig. 7 Inverted results using the IGWO based on noiseless forward modeling data from model B. **a** The measured apparent resistivity and phase and the predicted apparent resistivity and phase using the IGWO. **b** The search area, inversion solution and true model

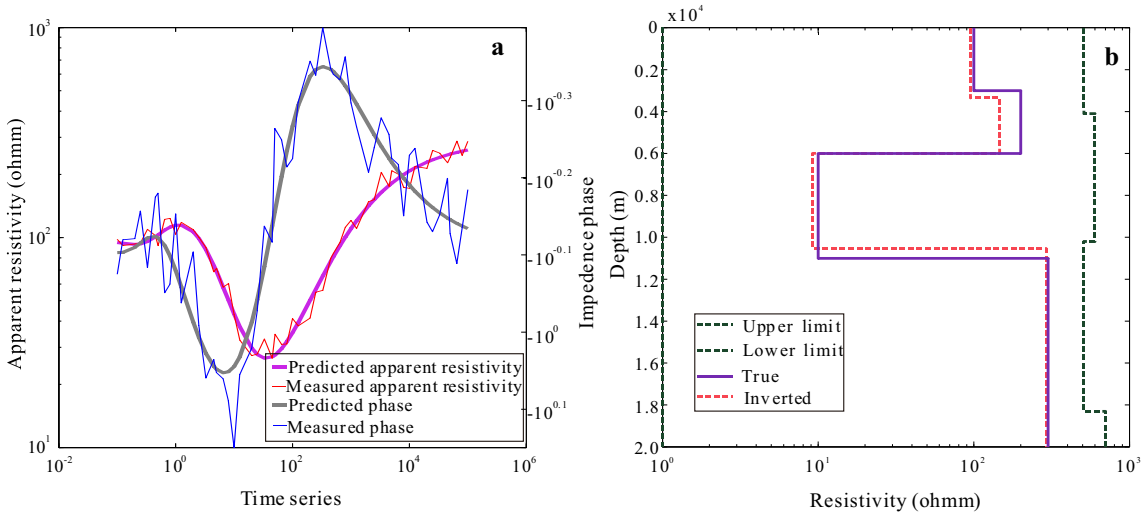

Fig. 8 Inverted results using the IGWO based on the data from model B with 10% noise. **a** The noisy measured apparent resistivity and phase and the predicted apparent resistivity and phase using the IGWO. **b** The search area, inversion solution and true model

Multi-extrema function tests

Three typical multi-extrema functions are chosen to evaluate the rationality of the IGWO. In every test, the grey wolf population $N = 5$. The three mathematical formulations are as follows:

$$F_1 = x^2 - 2\cos(2\pi x) + 2, -1000 \le x \le 1000, \quad (12)$$

$$F_2 = x^2 + y^2, -500 \le x, y \le 500, \quad (13)$$

$$F_3 = 0.5 + \left(\sin\left(\sqrt{x^2 + y^2 + z^2}\right)^2 - 0.5\right) / \left(1 + 0.0001 * \left(x^2 + y^2 + z^2\right)^2\right)^2 \quad (14)$$
$$-2000 \le x, y, z \le 2000,$$

Details about those functions and corresponding comparison results are depicted in Table 1.

The fitness behaviors of the GWO and IGWO in the above tests are exhibited in Fig. 4 for further verification of the high efficiency of the IGWO.

The results of the above tests reveal that the IGWO outperforms the GWO in terms of the number of iterations

Table 2 Electrical properties of the models, search space and results in the inversion of MT data by the IGWO

Model	Parameters	Iterations	True value	Search space		Estimated value	
				Minimum	Maximum	Noise-free	10% noise
Model A	ρ_1 (Ωm)	100	100	10	4010	105.3	82.68
	ρ_2 (Ωm)	100	1.5	0	300	1.462	1.509
	ρ_3 (Ωm)	100	50	10	2010	50.01	50.41
	h_1(m)	100	1000	100	4100	993.4	1034
	h_2(m)	100	100	10	410	97.82	99.48
Model B	ρ_1 (Ωm)	150	100	10	510	100.6	95.10
	ρ_2 (Ωm)	150	200	0	600	159.4	146.4
	ρ_3 (Ωm)	150	10	10	510	10.14	9.214
	ρ_4 (Ωm)	150	300	0	700	300.7	291.2
	h_1(m)	150	3000	100	4100	2845	3343
	h_2(m)	150	3000	100	6100	3190	2647
	h_3(m)	150	5000	100	8100	5047	4542

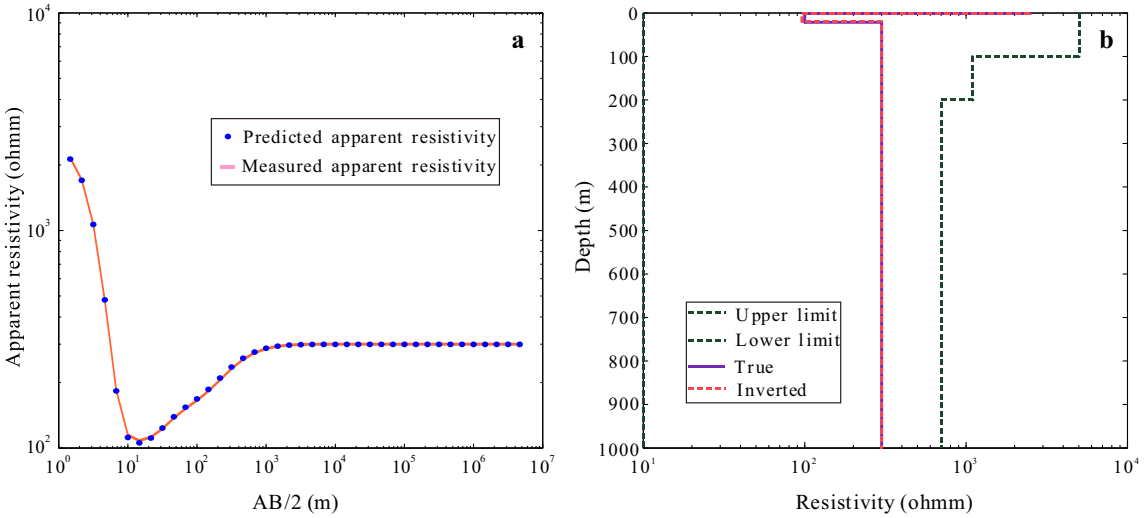

Fig. 9 Inverted results using the IGWO based on noiseless forward modeling data from model C. **a** The measured apparent resistivity and the predicted apparent resistivity using the IGWO. **b** The search area, inversion solution and true model

required to obtain an optimal solution, as exhibited in Table 1 and an improvement in misfit situations, as shown in Fig. 4.

IGWO for geophysical inversion

For geoelectrical data inversion, we focus on the thickness and the resistivity value of each layer of the geoelectrical models. The parameter vector is described as $\boldsymbol{x} = \{x_1, x_2, \ldots, x_{2m-1}\}$, where m is the number of layers; we assume that the population of the pack is N, and the location of each wolf is $\boldsymbol{x}_i = \{x_{i1}, x_{i2}, \ldots, x_{i(2m-1)}\}$. For each grey wolf, the objective function value using MT, DC resistivity and IP methods can be calculated, respectively, as follows:

$$\begin{cases} \Psi_{\mathrm{MT}} = \frac{1}{2}\sum_{i=1}^{n}\left(\frac{\rho_{ci}-\rho_{ai}}{\rho_{ai}}\right)^2 + \frac{1}{2}\sum_{i=1}^{n}\left(\frac{\varphi_{ci}-\varphi_{ai}}{\varphi_{ai}}\right)^2 \\ \Psi_{\mathrm{DC}} = \sum_{i=1}^{n}\left(\frac{\rho_{ci}-\rho_{ai}}{\rho_{ai}}\right)^2 \\ \Psi_{\mathrm{IP}} = \frac{1}{2}\sum_{i=1}^{n}\left(\frac{\rho_{ci}-\rho_{ai}}{\rho_{ai}}\right)^2 + \frac{1}{2}\sum_{i=1}^{n}\left(\frac{\eta_{ci}-\eta_{ai}}{\eta_{ai}}\right)^2 \end{cases}, \quad (15)$$

where ρ_c, ρ_a, φ_c, φ_a, η_c and η_a indicate the predicted apparent resistivity, the measured apparent resistivity, the predicted phase, the measured phase, the predicted apparent chargeability, and the measured apparent chargeability, respectively, and k indicates the length of the measured data. The first and third cases in Eq. (15) are treated as the resistivity and phase and resistivity and chargeability,

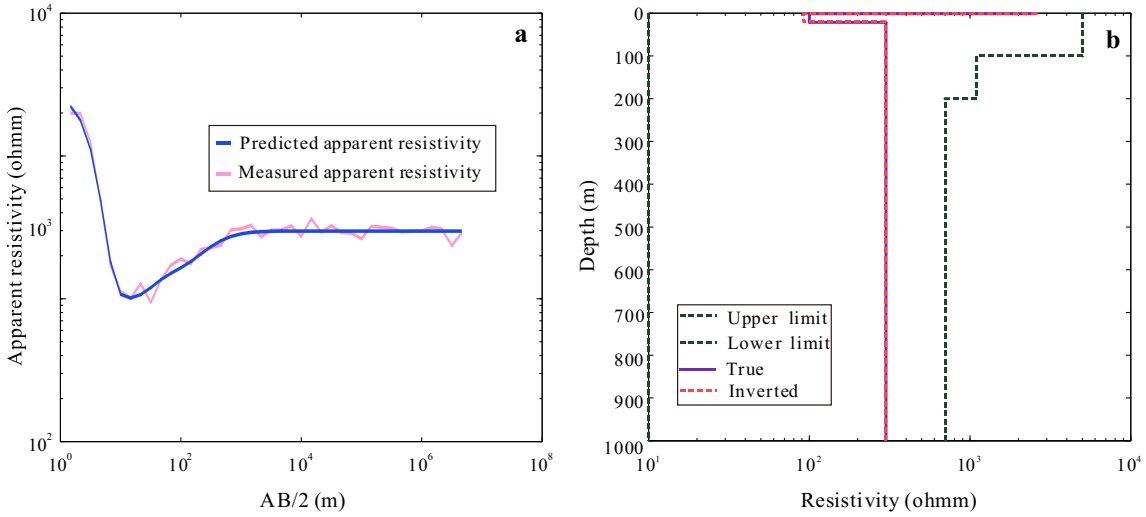

Fig. 10 Inverted results using the IGWO based on the data from model C with 10% noise. **a** The noisy measured apparent resistivity and the predicted apparent resistivity using the IGWO. **b** The search area, inversion solution and true model

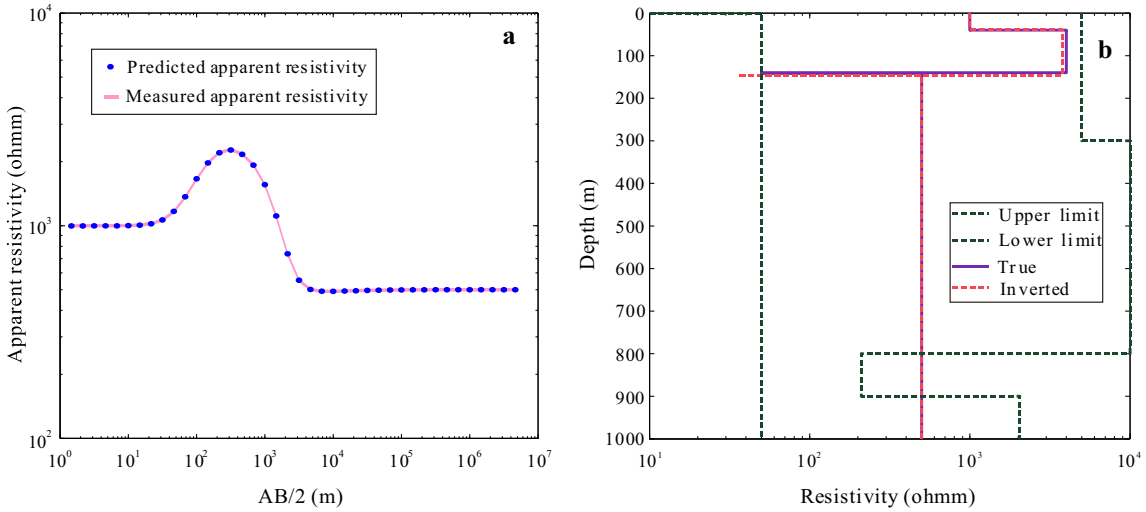

Fig. 11 Inverted results using the IGWO based on noiseless forward modeling data from model D. **a** The measured apparent resistivity and the predicted apparent resistivity using the IGWO. **b** The search area, inversion solution and true model

respectively, of joint inversion (Vozoff and Jupp 1975; Lines et al. 1988; Raiche 1985).Taking MT data as an example, the IGWO procedure for the inversion is proposed as follows:

1. Initialize the population N of the grey wolves, the number of iterations $t_{\max}$, $\boldsymbol{A}$, $\boldsymbol{C}$, and $\boldsymbol{a}$;
2. Initialize the location vector $\boldsymbol{x}_i$, and load the measured apparent resistivity ρ_a and phase φ_a;
3. Compute the corresponding fitness values, and initialize alpha, beta and delta;
4. Update the position of omegas using Eqs. (10) and (11); compute the fitness values of all updated location vectors for all the wolves; update alpha, beta and delta; and update $\boldsymbol{a}$, $\boldsymbol{A}$, and $\boldsymbol{C}$;
5. When the current iteration $t > t_{\max}$, end the iteration;
6. Return the position of alpha $\boldsymbol{x}_\alpha$ as the inverse result.

Synthetic data

MT, DC and IP data sets over three-layered and four-layered models are inverted to test the performances of the IGWO. Moreover, the noise-contaminated data sets perturbed by a 10% Gaussian noise are also inverted. Furthermore, a very wide searching area is designed in the tests below to prove the robustness of the IGWO.

For three-layered models, the grey wolf population $N = 30$ and the maximum iteration $t_{\max} = 100$. For four-layered

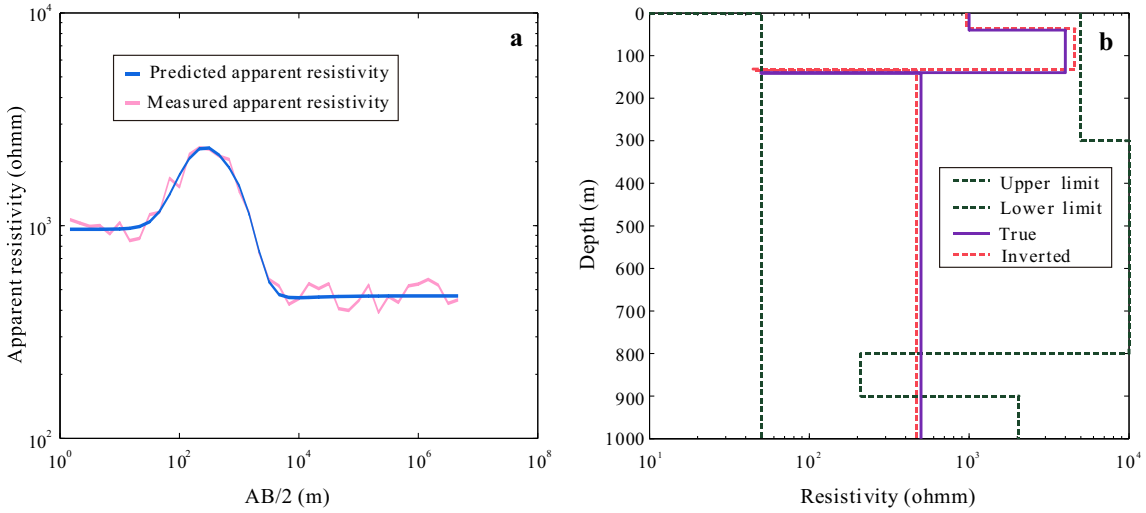

Fig. 12 Inverted results using the IGWO based on the data from model D with 10% noise. **a** The noisy measured apparent resistivity and the predicted apparent resistivity using the IGWO. **b** The search area, inversion solution and true model

Table 3 Electrical properties of the models, search space and results in the inversion of DC resistivity data by the IGWO

Model	Parameters	Iterations	True value	Search space		Estimated value	
				Minimum	Maximum	Noise-free	10% noise
Model C	ρ_1 (Ωm)	100	2500	10	5010	2463	2585
	ρ_2 (Ωm)	100	100	10	1100	96.23	91.98
	ρ_3 (Ωm)	100	300	0	700	299.4	297.6
	h_1(m)	100	1.5	0	100	1.514	1.514
	h_2(m)	100	20	0	100	18.07	18.03
Model D	ρ_1 (Ωm)	150	1000	10	5010	997.9	960.9
	ρ_2 (Ωm)	150	4000	0	10,000	3768	4593
	ρ_3 (Ωm)	150	50	10	210	35.69	44.50
	ρ_4 (Ωm)	150	500	50	2050	499.9	467.0
	h_1(m)	150	40	0	300	38.81	37.20
	h_2(m)	150	100	0	500	106.8	94.47
	h_3(m)	150	1.5	0	100	1.008	2.525

models, the grey wolf population $N = 60$ and the maximum iteration t_{max} = 150.

Magnetotelluric sounding

We consider two MT models: model A is an H-type geoelectrical structure with three layers, and the second layer is a relatively conductive thin layer; model B is a KH-type geoelectrical structure with four layers. There is approximately 200–10,000% searching area departure from the real values in model A and 66–2500% in model B. The results of the tests on the synthetic and noise-contaminated MT data are illustrated in Figs. 5, 6, 7 and 8. More information on the models and results of the inversions is given in Table 2.

DC resistivity

Two models are provided using the DC resistivity method: model C and model D. Model C consists of a resistive thin layer, and model D consists of a conductive thin layer. There is approximately 100–3333% searching area departure from the real values in model C and 125–3333% in model D. The results of tests on the synthetic and contaminated DC resistivity data are illustrated in Figs. 9, 10, 11 and 12. More information on the models and results of the inversions is given in Table 3.

Induced polarization (IP)

Two models are considered using the IP method: model E and model F. Model E simulates a silver mineral with a

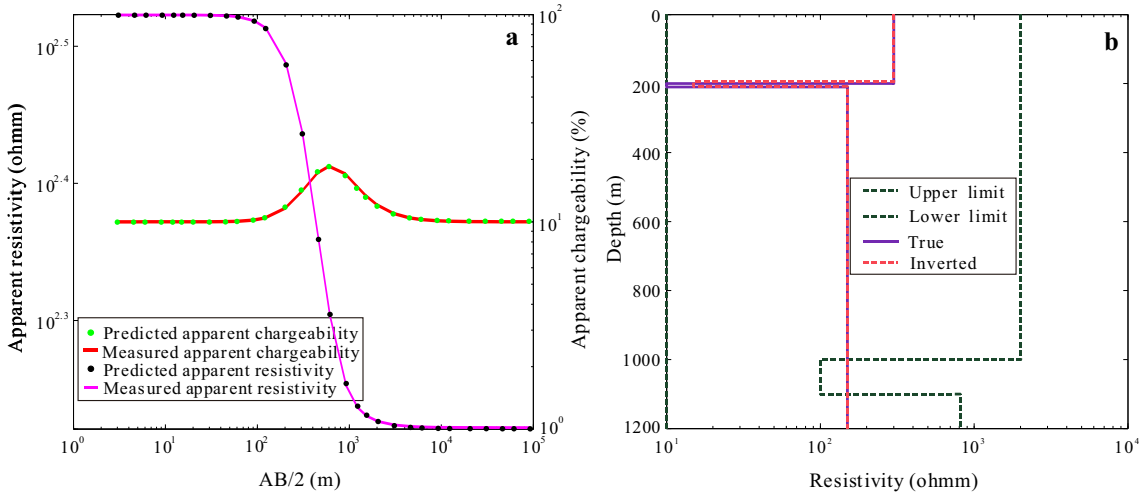

Fig. 13 Inverted results using the IGWO based on noiseless forward modeling data from model E. **a** The measured apparent resistivity and chargeability and the predicted apparent resistivity and chargeability using the IGWO. **b** The search area, inversion solution and true model

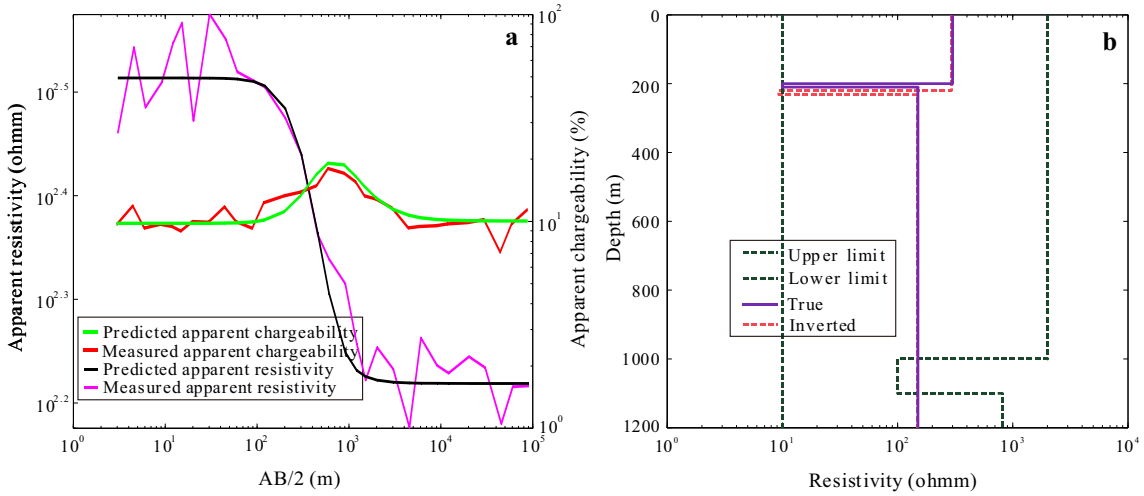

Fig. 14 Inverted results using the IGWO based on the data from model E with 10% noise. **a** The noisy measured apparent resistivity and chargeability and the predicted apparent resistivity and chargeability using the IGWO. **b** The search area, inversion solution and true model

low-resistivity and high-chargeability thin layer, and model F simulates a non-mineralized rock with a high-resistivity and low-chargeability thin layer. There is approximately 83–500% searching area departure from the real values in model E and 125–1000% in model F. The results of tests on the synthetic and contaminated IP data are illustrated in Figs. 13, 14, 15 and 16. More information on the models and results of the inversions is given in Table 4.

Comparisons with other algorithms

The results of the IGWO based on models A, B, C and D are contrasted with the PSO and the SA algorithm for further verification of the accuracy and efficiency of the IGWO. We set inverted parameters (search space and maximum iteration) in the IGWO to be the same as those in the PSO and SA. For models A and C, the initial model number $N = 30$ and the maximum iteration $t_{\max} = 100$. For models B and D, the initial model number $N = 60$ and the maximum iteration $t_{\max} = 150$. In the SA algorithm, the temperature T equation for the iterative annealing process is: $T(k) = 0.5 \times 0.99^k$. Additionally, the acceptance probability $P(\Delta E) = \exp\left(-\frac{\Delta E}{T}\right)$. ΔE indicates the objective difference.

The search space and the experimental results are provided in Table 5. In addition, the relative errors between the predicted data inverted by SA, PSO and IGWO algorithms and the measured data are depicted in Table 6.

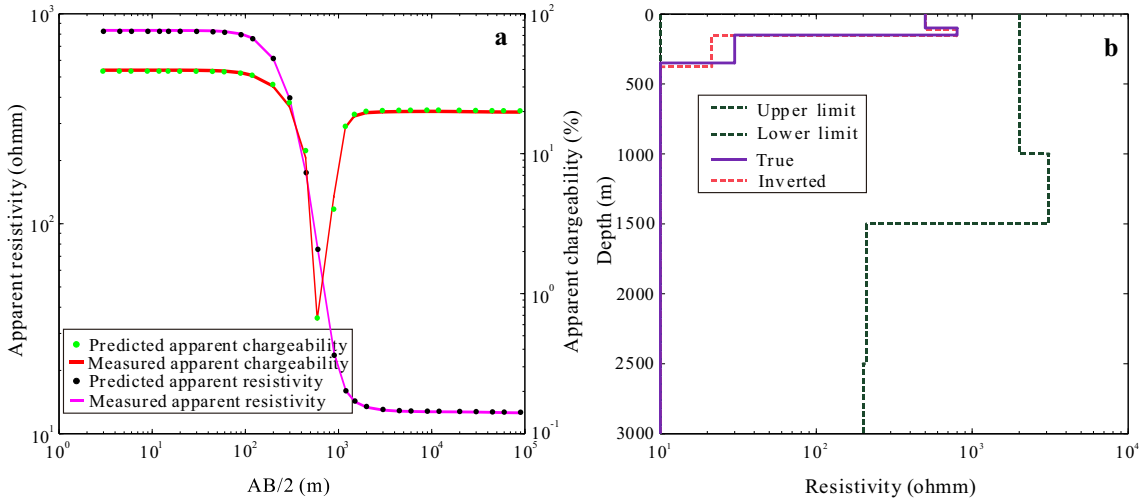

Fig. 15 Inverted results using the IGWO based on noiseless forward modeling data from model F. **a** The measured apparent resistivity and chargeability and the predicted apparent resistivity and chargeability using the IGWO. **b** The search area, inversion solution and true model

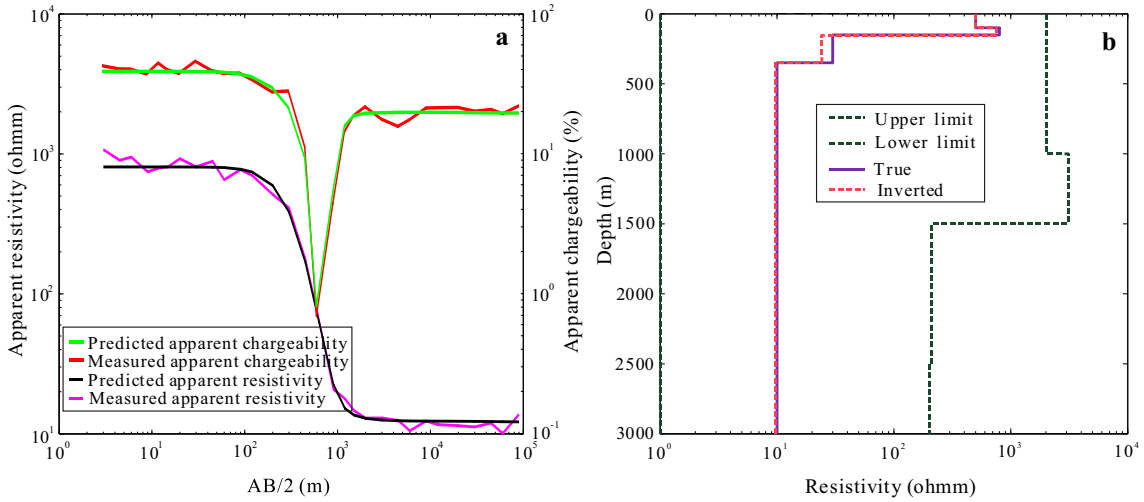

Fig. 16 Inverted results using the IGWO based on the data from model F with 10% noise. **a** The noisy measured apparent resistivity and chargeability and the predicted apparent resistivity and chargeability using the IGWO. **b** The search area, inversion solution and true model

Comparisons of fitness behaviors between the SA, PSO and IGWO are exhibited in Fig. 17.

We can clearly see that the IGWO and PSO outperform the SA in terms of the accuracy of the finial inverted results and their convergence speeds. The typical characteristics of the SA, PSO and IGWO are quite well illustrated in the convergence curves in Fig. 17. For the IGWO and PSO, the misfit function values in Fig. 17 always sharply decay at the very beginning of the iterations and generally quickly derive a small number at the next iteration. For SA, the objective values are all greater than those in the IGWO and PSO. Tables 5 and 6 and Fig. 17 reveal that the IGWO and PSO have better performances than the SA in terms of those improved misfit situations.

The CPU time (a CPU-i5 2540 M with 2.60-GHz clock speed) needed for one iteration and the number of iterations required to obtain an acceptable solution in the SA, PSO, GWO and IGWO inversions are shown in Table 7. Table 7 indicates that the IGWO is more time consuming than the PSO, SA and the original GWO. Generally, the PSO, GWO and IGWO require fewer iterations than does SA to obtain an acceptable solution.

Field data

For further investigation and evaluation of the performance and robustness of the IGWO algorithm, the observed MT data acquired at Caosiyao Village of Ulanqab City in the

Table 4 Electrical properties of the models, search space and results in the inversion of IP data by the IGWO

Model	Parameters	Iterations	True value	Search space		Estimated value	
				Minimum	Maximum	Noise-free	10% noise
Model E	ρ_1 (Ωm)	100	300	10	2010	299.9	294.2
	ρ_2 (Ωm)	100	10	0	100	14.96	9.320
	ρ_3 (Ωm)	100	150	10	810	149.6	148.8
	h_1(m)	100	200	0	1000	194.7	219.4
	h_2(m)	100	10	0	100	13.35	12.23
	η_1(%)	100	10	0	100	9.968	9.619
	η_2(%)	100	60	0	100	62.28	58.10
	η_3(%)	100	10	0	100	10.05	9.866
Model F	ρ_1 (Ωm)	150	500	10	2010	500.3	498.1
	ρ_2 (Ωm)	150	800	100	3100	793.1	750.2
	ρ_3 (Ωm)	150	30	10	210	21.34	24.19
	ρ_4 (Ωm)	150	10	0	200	10.00	9.783
	h_1(m)	150	100	0	1000	111.6	98.26
	h_2(m)	150	50	0	500	44.72	54.89
	h_3(m)	150	200	0	1000	220.4	193.0
	η_1(%)	150	40	0	100	39.37	38.37
	η_2(%)	150	5	0	100	1.145	6.072
	η_3(%)	150	30	0	100	27.43	32.63
	η_4(%)	150	20	0	100	20.43	19.27

Table 5 Search space and results of the inversions using the MT and DC methods based on the SA, PSO and IGWO algorithms

Model	Parameters	True value	Search space	Estimated value		
				SA	PSO	IGWO
Model A	ρ_1 (Ωm)	100	0–200	109.4	101.7	99.67
	ρ_2 (Ωm)	1.5	0–100	1.190	1.248	1.691
	ρ_3 (Ωm)	50	0–100	54.75	49.97	50.03
	h_1(m)	1000	0–2000	1049	1003	995.5
	h_2(m)	100	0–200	88.84	82.85	113.4
Model B	ρ_1 (Ωm)	100	0–200	102.2	99.17	99.75
	ρ_2 (Ωm)	200	0–400	201.8	274.7	182.9
	ρ_3 (Ωm)	10	0–100	12.03	10.91	10.92
	ρ_4 (Ωm)	300	0–600	283.8	299.8	301.1
	h_1(m)	3000	0–6000	3577	3019	2860
	$h_2(m)$	3000	0–6000	3349	2788	3024
	h_3(m)	5000	0–10,000	8177	5529	5504
Model C	ρ_1 (Ωm)	2500	0–5000	3008	2385	2466
	ρ_2 (Ωm)	100	0–200	119.4	124.7	95.56
	ρ_3 (Ωm)	300	0–600	292.2	303.5	300.7
	h_1(m)	1.5	0–100	1.352	1.474	1.517
	h_2(m)	20	0–100	25.28	41.83	18.06
Model D	ρ_1 (Ωm)	1000	0–2000	925.3	994.2	998.3
	ρ_2 (Ωm)	4000	0–8000	3864	4219	3952
	ρ_3 (Ωm)	50	0–100	39.97	92.28	98.10
	ρ_4 (Ωm)	500	0–1000	529.6	498.7	499.8
	h_1(m)	40	0–100	40.19	39.21	39.62
	h_2(m)	100	0–200	74.82	96.40	101.4
	h_3(m)	1.5	0–100	11.19	4.172	2.980

Table 6 The relative errors between the predicted data inverted by the SA, PSO and IGWO algorithms and the measured data

Model	Relative errors		
	SA (%)	PSO (%)	IGWO (%)
Model A	1.98	0.0428	0.0608
Model B	2.01	0.0475	0.0899
Model C	3.05	1.69	0.219
Model D	1.04	1.33	0.0554

Inner Mongolia Autonomous Region of northern China are analyzed using the IGWO algorithm. The MT survey was conducted for a total of 130 stations and divided into 8 lines that extend from northwest to southeast. The original data from the fifteenth station on the fourth line are inversed using the IGWO. The inverted results of the IGWO algorithm for the observed MT data are illustrated in Fig. 18. The relative error between the predicted data and the observed data is 4.225%.

Figure 18a illustrates that the predicted apparent resistivity fits the measured apparent resistivity quite well. Beneath the sounding station, resistivity values tend to increase with depth. Figure 18b shows the convergence behavior in the iterative process of the IGWO. The objective function values in Fig. 18b sharply decay during the first 20 iterations and generally quickly derive a small number during the following 80 iterations. Figure 18c depicts the inverted solutions from the IGWO and OCCAM by WinGLink. The inverted solution generally conforms to the results obtained using OCCAM as well as the interpretation results by our previous work shown on the right side of Fig. 18c.

Generally, the clay cap layer possesses a very low-resistivity value of approximately 100 Ωm at depths of 0–286 m above the surface. The second layer is a low-resistivity layer (2000 Ωm) at depths of 0–4873 m below the surface. Below the two low-resistivity layers, resistivity tends to sharply increase to approximately 20,000 Ωm, which is interpreted as the zone of granitic batholith.

Conclusions

This paper proposes an emerging geophysical inversion algorithm named the IGWO. The GWO algorithm is a recently developed bionic algorithm inspired by the social rank and prey-seeking behaviors of grey wolves in nature. The mathematical theory of trailing, surrounding, and assaulting prey can be applied to the inverse problem of geoelectrical data. We made improvements to the

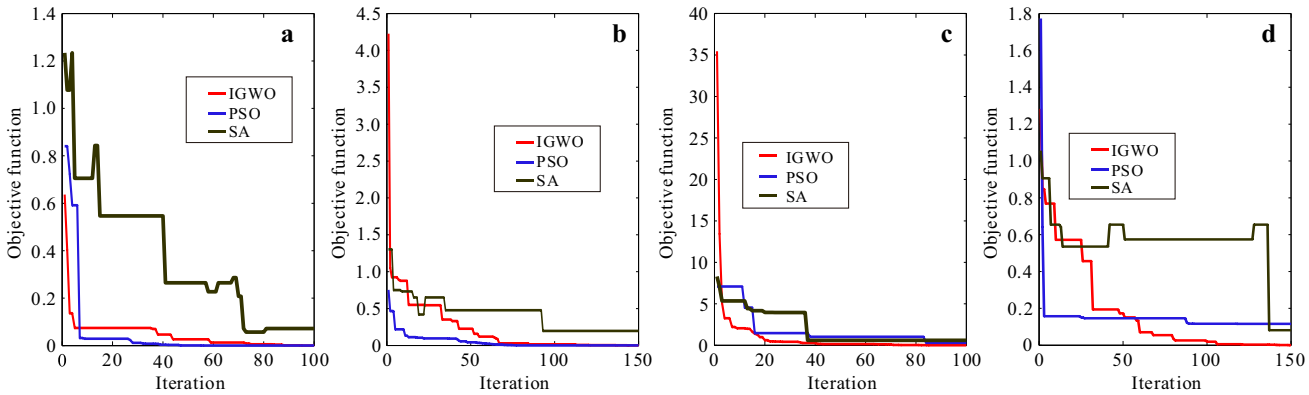

Fig. 17 Comparisons of fitness behaviors between the SA, PSO and IGWO algorithms. **a** Objective functions in the iterative process based on model A. **b** Objective functions in the iterative process based on model B. **c** Objective functions in the iterative process based on model C. **d** Objective functions in the iterative process based on model D

Table 7 CPU time needed for one iteration and the number of iterations required to obtain an acceptable solution in the SA, PSO, GWO and IGWO inversions

Model	CPU time (s)				Number of iterations required			
	SA	PSO	GWO	IGWO	SA	PSO	GWO	IGWO
Model A	0.2344	0.1563	0.2188	0.2031	73	48	40	38
Model B	0.3281	0.2969	0.4219	0.4375	69	51	50	54
Model C	0.0625	0.0781	0.1406	0.1719	45	34	30	36
Model D	0.0938	0.1094	0.3906	0.4063	51	21	14	16

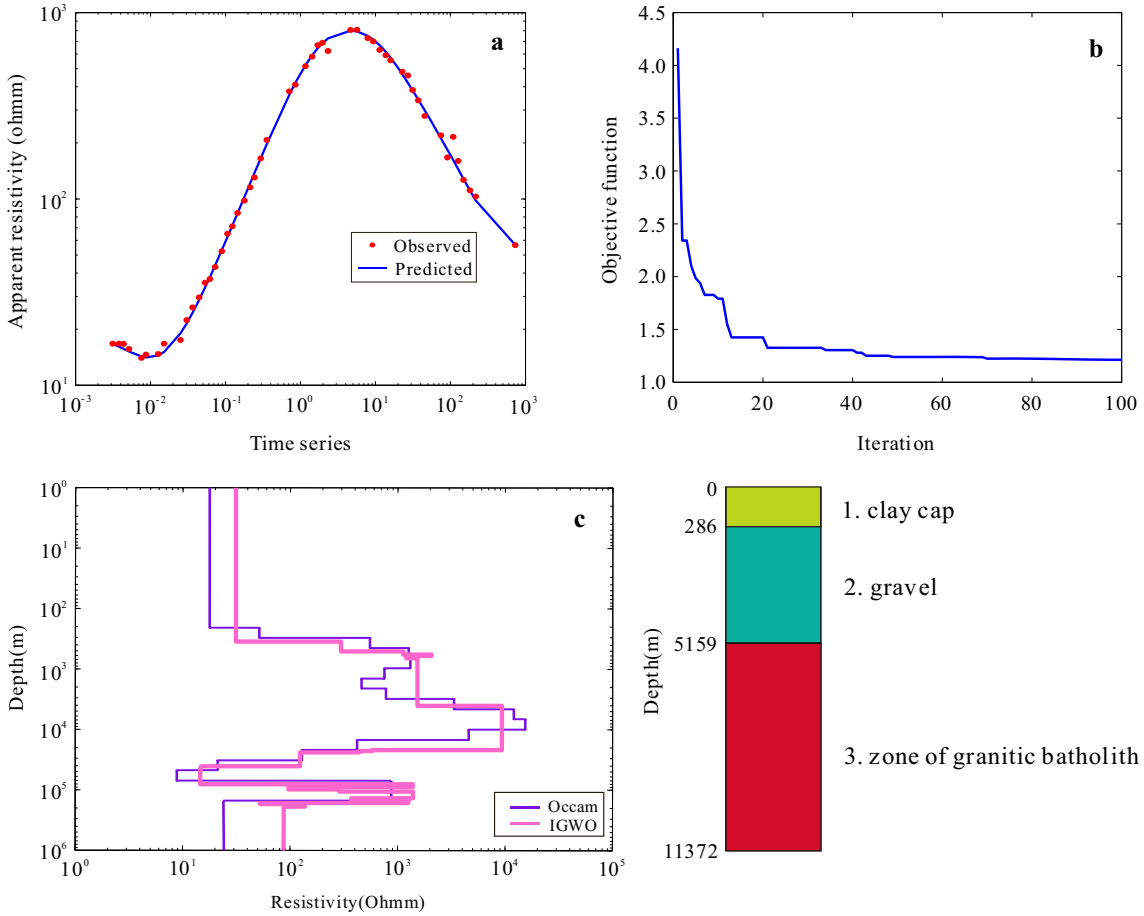

Fig. 18 A field data example. **a** The measured and predicted apparent resistivity of the IGWO. **b** The fitness behavior of the IGWO. **c** Inversion results using the IGWO and OCCAM by WinGLink. Also shown is the inverse result from the previous work

convergence factor and the location updating strategy of the original GWO algorithm. This modified GWO algorithm was named the IGWO. In the procedure of inversion, we adopted a quite wide searching space. The effectiveness and robustness of the IGWO were also tested on the noiseless, contaminated, and observed data. For verification, comparisons were made between the inverted results of the PSO, SA and IGWO algorithm. Contrastive tests demonstrated that the IGWO and PSO perform much better in counterpoising the exploration and exploitation in the iterations than SA. In contrast to PSO, the IGWO can acquire more accurate results and provides more improved misfit values.

We have shown that the IGWO can be applied to geoelectrical inverse problems. The high performance, efficiency, and accuracy and the satisfactory convergence characteristics of the IGWO algorithm are sufficiently illustrated in this paper.

Acknowledgements This research was supported by the National Natural Science Foundation of China (NSFC) (No. 41574067) and the National Programs for High Technology Research and Development of China (No. 2012AA09A404). The authors sincerely thank Yang Hao, Wang Xuemei and Yuan Wenxiu for their constructive suggestions and encouraging comments.

Compliance with ethical standards

Conflict of interest On behalf of all authors, the corresponding author states that there are no conflicts of interest.

References

Chahar V, Kumar D (2017) An astrophysics-inspired Grey wolf algorithm for numerical optimization and its application to engineering design problems. Adv Eng Softw 112:231–254

Chen S, Wang S, Zhang Y (2005) Ant colony optimization for the seismic nonlinear inversion/SEG technical program expanded abstracts 2005. Soc Explor Geophys 24(1):1732–1734

Davis P (1993) Levenberg-marquart methods and nonlinear estimation. Siam News 26(6):1–12

Dorigo M, Stützle T (2003) The ant colony optimization metaheuristic: algorithms, applications, and advances. In: Glover F, Kochenberger GA (eds) Handbook of metaheuristics. International series in operations research & management science, vol

57. Springer, Boston, MA, pp 250–285 https://doi.org/10.1007/0-306-48056-5_9
Dos Santos Coelho L, Alotto P (2008) Global optimization of electromagnetic devices using an exponential quantum-behaved particle swarm optimizer. IEEE Trans Magn 44(6):1074–1077
Dosso SE, Oldenburg DW (1991) Magnetotelluric appraisal using simulated annealing. Geophys J Int 106(2):379–385
Heidari AA, Pahlavani P (2017) An efficient modified grey wolf optimizer with Lévy flight for optimization tasks. Appl Soft Comput 60:115–134
Jadhav AN, Gomathi N (2017) WGC: hybridization of exponential grey wolf optimizer with whale optimization for data clustering. Alex Eng J. https://doi.org/10.1016/j.aej.2017.04.013
Kamboj VK, Bath SK, Dhillon JS (2016) Solution of non-convex economic load dispatch problem using Grey Wolf Optimizer. Neural Comput Appl 27(5):1301–1316
Krishnanand KN (2007) Glowworm swarm optimization: a multimodal function optimization paradigm with applications to multiple signal source localization tasks/2013 international conference on computing, networking and communications (ICNC). IEEE Comput Soc 2:600–605
Krishnanand KN, Ghose D (2006) Glowworm swarm based optimization algorithm for multimodal functions with collective robotics applications. Multiagent Grid Syst 2(3):209–222
Lines LR, Schultz AK, Treitel S (1988) Cooperative inversion of geophysical data. Geophysics 53(3):8–20
Mikki S, Kishk AA (2005) Investigation of the quantum particle swarm optimization technique for electromagnetic applications/antennas and propagation society international symposium. IEEE 2:45–48
Mirjalili S (2015a) The ant lion optimizer. Adv Eng Softw 83:80–98
Mirjalili S (2015b) How effective is the Grey Wolf optimizer in training multi-layer perceptrons. Appl Intell 43(1):150–161
Mirjalili S, Mirjalili SM, Lewis A (2014) Grey wolf optimizer. Adv Eng Softw 69:46–61
Mirjalili S, Mirjalili SM, Hatamlou A (2016) Multi-verse optimizer: a nature-inspired algorithm for global optimization. Neural Comput Appl 27(2):495–513
Mittal N, Singh U, Sohi BS (2016) Modified grey wolf optimizer for global engineering optimization. Appl Comput Intell Soft Comput 2016:1–16
Mo X, Li X, Zhang Q (2016) The variation step adaptive Glowworm swarm optimization algorithm in optimum log interpretation for reservoir with complicated lithology. In: 12th international conference on natural computation, fuzzy systems and knowledge discovery (ICNC-FSKD), 2016. IEEE, 1044–1050
Mohamed AAA, El-Gaafary AAM, Mohamed YS et al. (2015) Design static VAR compensator controller using artificial neural network optimized by modify grey wolf optimization. In International joint conference on neural networks. IEEE, 1–7
Muangkote N, Sunat K, Chiewchanwattana S., 2014. An improved grey wolf optimizer for training q-Gaussian radial basis functional-link nets. In: Computer science and engineering conference. IEEE, 209–214
Muro C, Escobedo R, Spector L et al (2011) Wolf-pack (Canis lupus) hunting strategies emerge from simple rules in computational simulations. Behav Proc 88(3):192–197
Nabighian MN, Asten MW (2002) Metalliferous mining geophysics—state of the art in the last decade of the 20th century and the beginning of the new millennium. Geophysics 67(3):964–978
Pan WT (2012) A new fruit fly optimization algorithm: taking the financial distress model as an example. Knowl Based Syst 26:69–74
Parolai S, Picozzi M, Richwalski SM et al. (2005) Joint inversion of phase velocity dispersion and H/V ratio curves from seismic noise recordings using a genetic algorithm, considering higher modes. Geophys Res Lett 32(1):67–106
Raiche AP (1985) The joint use of coincident loop transient electromagnetic and Schlumberger sounding to resolve layered structures. Geophysics 50(10):1618–1627
Rashedi E, Nezamabadi-Pour H, Saryazdi S (2009) GSA: a gravitational search algorithm. Inf Sci 179(13):2232–2248
Sen MK, Stoffa PL (1992) Rapid sampling of model space using genetic algorithms: examples from seismic waveform inversion. Geophys J Int 108(1):281–292
Shaw R, Srivastava S (2007) Particle swarm optimization: a new tool to invert geophysical data. Geophysics 72(2):F75–F83
Shi XM, Wang JY, Zhang SY et al (2000) Multiscale genetic algorithm and its application in magnetotelluric sounding data inversion. Chin J Geophys Chin Ed 43(1):122–130
Simpson F, Bahr K (2005) Practical magnetotellurics. Cambridge University Press, Cambridge
Smith ML, Franklin JN (1969) Geophysical application of generalized inverse theory. J Geophys Res 74(10):2783–2785
Song X, Tang L, Zhao S et al (2015) Grey wolf optimizer for parameter estimation in surface waves. Soil Dyn Earthq Eng 75:147–157
Sulaiman MH, Mustaffa Z, Mohamed MR et al (2015) Using the gray wolf optimizer for solving optimal reactive power dispatch problem. Appl Soft Comput 32:286–292
Vozoff K, Jupp DLB (1975) Joint inversion of geophysical data. Geophys J Roy Astron Soc 42(3):977–991
Wang J, Tan Y (2005) 2-D MT inversion using genetic algorithm. J Phys Conf Ser 12(1):165 **(IOP Publishing)**
Wang S, Liu Y, Wang J (2009) Lecture on non-linear inverse methods in geophysical data (9)—ant colony optimization. Chin J Eng Geophys 6(2):131–136
Wang R, Yin C, Wang M et al (2012) Simulated annealing for controlled-source audio-frequency magnetotelluric data inversion. Geophysics 77(2):E127–E133
Yang XS (2010) A new metaheuristic bat-inspired algorithm, nature inspired cooperative strategies for optimization (NISCO2010), vol 284. Springer, Berlin, pp 65–74
Yang XS (2011) Bat algorithm for multi-objective optimisation. Int J Bio Inspired Comput 3(5):267–274
Yang XS, Hossein Gandomi A (2012) Bat algorithm: a novel approach for global engineering optimization. Eng Comput 29(5):464–483
Yang H, Wang JL, Wu JS et al (2002) Constrained joint inversion of magneto-telluric and seismic data using simulated annealing algorithm. Chin J Geophys 45(5):764–776
Zhdanov MS (2010) Electromagnetic geophysics: notes from the past and the road ahead. Geophysics 75(5):75A49–75A66
Zhu A, Xu C, Li Z et al (2015) Hybridizing grey wolf optimization with differential evolution for global optimization and test scheduling for 3D stacked SoC. J Syst Eng Electron 26(2):317–328